3-2013

How Rigid is a Rigid Plate? Geodetic Constraint from the TrigNet CGPS Network, South Africa

Rocco Malservisi
University of South Florida, rocco@usf.edu

Urs Hugentobler
Technische Universität München

Richard Wonnacott
National Geo-Spatial Inormation, Mowbray, South Africa

Matthias Hackl
Ludwig-Maximilians Universität

Geophysical Journal International

Geophys. J. Int. (2013) **192,** 918–928 doi: 10.1093/gji/ggs081

How rigid is a rigid plate? Geodetic constraint from the TrigNet CGPS network, South Africa

Rocco Malservisi,[1] Urs Hugentobler,[2] Richard Wonnacott[3] and Matthias Hackl[4]

[1] *Department of Geology, University of South Florida,* 4202 *E. Fowler Ave.,* SCA528, *Tampa, FL* 33620, *USA. E-mail: rocco@usf.edu*
[2] *Institute for Astronomical and Physical Geodesy, Technische Universität München, Munich, Germany.*
[3] *Chief Directorate: National Geo-spatial Information, Mowbray, South Africa.*
[4] *Department of Earth and Environmental Sciences, Ludwig Maximilians-Universität, Munich, Germany*

Accepted 2012 November 21. Received 2012 November 20; in original form 2012 April 9

SUMMARY

Rigidity and continuity of the Nubia plate is a fundamental assumption for the kinematic description, the dynamic implications of its interaction with surrounding plates and ultimately an important constraint to the geodynamics processes involved in continental lithospheric rupture. Geophysical, neotectonic and geodynamics considerations suggest the possibility that the Nubia plate is not completely rigid but could be undergoing internal deformation due to the southward propagation of the East African Rift. Here, we utilize the South African TrigNet geodetic network to evaluate the amount of internal deformation within the South African region and the possibility of motion between South Africa and the rest of the African continent. Our results show that the South African region behaves rigidly, with deformation of the order of 1 nanostrain yr^{-1} or less. The analysis shows some higher strain rates in the eastern region, and the presence of spatially correlated residuals in the Cape Town region and the region east of Johannesburg. Although not statistically significant, the spatial coherence of those residuals could indicate tectonic activity. A comparison of the Euler vector for the South African region with previously published Euler poles for the Nubia plate as well as the analysis of the residuals of Nubia sites with respect to a 'rigid' TrigNet are compatible with clockwise rotation of the South African block with respect to the African continent, consistent with a propagation of the East Africa Rift along the Okavango region.

Key words: Time series analysis; Reference systems; Plate motions; Intra-plate processes; Africa.

1 INTRODUCTION

The rigidity of plates is an important part of the plate tectonics paradigm and a necessary assumption for plate reconstructions and geodynamic modelling (e.g. McKenzie & Parker 1967; Le-Pichon 1968; Morgan 1968; DeMets *et al.* 1990; Sella *et al.* 2002). The assumption of rigid plate interiors is a useful but uncertain approximation, particularly in areas of slow rifting (Dixon *et al.* 1996; Gordon 1998; Hartnady 2002). The development of satellite geodesy and the possibility to measure with sufficient precision of the motions of points within plates allow an evaluation of rigidity on global and regional scales (Drewes 1982; Dixon 1991; Dixon *et al.* 1996; Sella *et al.* 2002; Plattner *et al.* 2007). In this paper, we use continuous GPS (CGPS) within the Nubia plate and in particular in South Africa to test the rigidity of the South African portion of the Kalahari craton, and of the Nubia plate. Many previous GPS-based studies of plate rigidity have been in the northern hemisphere, and hence are affected by glacial isostatic adjustment (GIA), the slow response to the lithosphere to past loading events from the last glaciation. This can impart a significant non-tectonic signal in the plate interior (e.g. Sella *et al.* 2007). One advantage of the current study is that the South Africa craton was not affected by Holocene glaciation, allowing us to better assess the limits to plate rigidity.

2 GEOLOGICAL BACKGROUND

The Nubia plate (sometimes referred as African plate) constitutes the largest part of the African continent. On the north (Fig. 1), the plate is affected by the collision with Eurasia along the Mediterranean margin (e.g. McClusky *et al.* 2003). The other boundaries are mainly extensional: on the west, the plate is bounded by the Mid-Atlantic Ridge; on the south by the South–West Indian ridge; and on the east by a more complex boundary that implies a transition from oceanic spreading in the Red Sea and Afar to continental rifting in the south (Ebinger 1989; Hartnady 1990; Stamps *et al.* 2008). The extensional regime in the east is accommodated along different branches of the East African Rift that breaks the African continent into two major plates: Nubia and Somalia. Here, plate motion is accommodated by a rift system propagating between cratonic blocks, creating a series of microplates accommodating the relative motion (Ebinger 1989; Hartnady 1990, 2002; Calais *et al.*

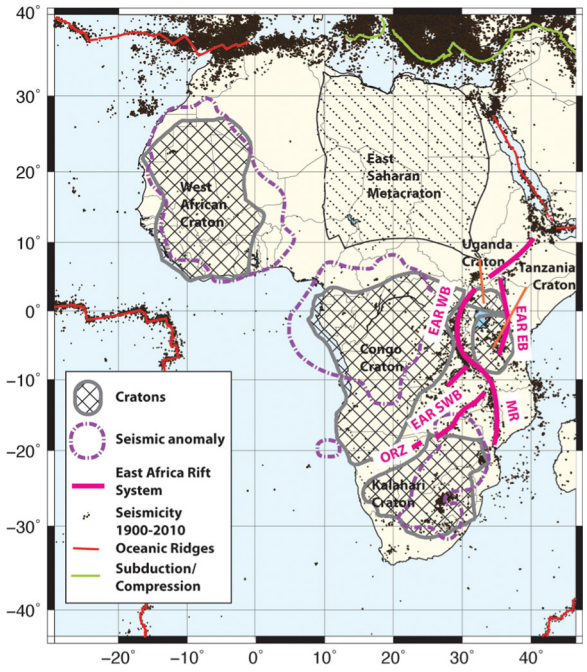

Figure 1. Africa continent tectonic setting. Cratons and Metacratons outline from fig. 1 of Begg *et al.* (2009). The cratons' root is also indicated by the +5 per cent seismic velocity anomaly in the layer 100–175 km from Begg *et al.* (2009) tomography (indicated by the dashed line). Ridges and subduction lines from http://www.ig.utexas.edu/research/projects/plates/data.htm (last accessed 21 December 2012). Seismicity from International Seismological Centre (2010). The thick red line delineates the different branches of the East Africa Rift (West Branch (EAR WB); East Branch (EAR EB); Lake Malawi Rift (MR); Southwest Branch (EAR SWB), including Luangwa rift and Okavango Rift Zone (ORZ)).

2006; Stamps *et al.* 2008). The complexity of the Nubia/Somalia boundary increases southward, perhaps due to the proximity to the rotation pole describing the Nubia–Somalia motion. Here, the deformation is probably accommodated by a broad deformation zone and the boundary between plates is not clearly defined (Gordon 1998; Hartnady 2002; Stamps *et al.* 2008).

The continental extent of the Nubia plate mainly comprises cratons assembled together during the formation of super-continents (at least Gondwana and possibly Rodina) and separated by old deformation belts (Dalziel *et al.* 2000; Kröner & Cordani 2003; Tohver *et al.* 2006; Begg *et al.* 2009)(Fig. 1). Preceding the breakup of Gondwana and the reactivation of the plate boundary along the current South Atlantic passive margin, these cratonic regions had a relatively long period of tectonic quiescence. The major events predating the opening of the South Atlantic Ocean may be recorded in the late Paleozoic orogeny of the Cape Fold Belt, but are much older in regions as the Kalahari shield (Andreoli *et al.* 1996). Recent plate reconstructions suggest some internal deformation, with relative motion along the major deformation belt during the Gondwana breakup (Reeves 1999; Reeves & De Wit 2000; DeWit *et al.* 2000; Reeves *et al.* 2004; Eagles 2007). How much of this internal deformation is still active is a key question, and the main focus of this paper.

From a geodynamics point of view, the East and South Africa Plateau, as well as the adjacent southeastern Atlantic Ocean basin, are characterized by anomalously elevated topography identified by Nyblade & Robinson (1994) as the African Superswell. This average ∼500 m of excess topography has generally been associated with dynamic support due to mantle convection and a broad zone of low seismic velocity rooted in the deep mantle, the African Superplume (Lithgow-Bertelloni & Silver 1998; Gurnis *et al.* 2000; Behn *et al.* 2004; Forte *et al.* 2010). Dynamic uplift due to thermal alteration by Cenozoic-/Mesozoic-plume-related activities has also been suggested for the Southern African Plateau (Nyblade & Sleep 2003). It has been suggested that the interaction of the African plate with one or multiple plumes played a major role in the rupture of the continental lithosphere, the development of the East African Rift and ultimately the detachment of the Somalian plate (Ebinger 1989; Ebinger *et al.* 1989; Ebinger & Sleep 1998). The presence of flood basalt (Erlank *et al.* 1984), extensive mafic dike swarms (Watkins *et al.* 1994; Milner *et al.* 1995) and kimberlites with associated magmatism (Smith *et al.* 1985) across the southern extent of the Africa Continent (Burke 1996) suggest that the same mechanism, at least in the past, could have been active in this region.

Previous geodetic work using the sparse GPS and DORIS network throughout Africa indicates that the Nubia plate is rigid within the measured uncertainties (few mm yr^{-1}) (Nocquet *et al.* 2006). However, other evidence suggests internal deformation, including seismicity (Reeves 1972; Scholz *et al.* 1976; Fairhead & Henderson 1977; Nyblade & Langston 1995; Hlatywayo 1997; Hartnady 1990; Midzi *et al.* 1999; Graham & Brandt 2000; Hartnady 2002), potential field (Modisi 2000; Modisi *et al.* 2000; Kinabo *et al.* 2007, 2008; Shemang & Molwalefhe 2011) and geomorphology (Gumbricht *et al.* 2001). These latter observations indicate the possibility of a propagation of the East African Rift System along a south-western branch in the Luangwa and Okavango rifts, and the presence of relative motions between the Kalahari and Congo Cratons. The locations of the TrigNet CGPS sites, mostly in the stable cratonic region of South Africa, provides a test of the plate rigidity assumption in a tectonically inactive region, and could detect relative motion between South Africa and the region to the north.

3 TRIGNET NETWORK AND DATA PROCESSING

TrigNet is a network of continuous GPS base stations deployed by the National Geo-Spatial Information (NGI, previously Chief Directorate: Survey and Mapping, Mowbray, South Africa) to provide data for surveyors and engineers for a wide variety of applications. The network consists of ∼65 continuously observing stations with an average distance of 200 km and local densifications (∼70 km) around Cape Town, Johannesburg and Durban (Figs 2 and 3 and Table 1). Data are freely available from the TrigNet web page [ftp://ftp.trignet.co.za (last accessed 21 December 2012)] and span a period between more than 10 yr for the oldest sites to few months for the most recent ones. Only sites with at least 1000 d of recording by June 2011 were used in this paper (the average time span is ∼5 yr, Fig. 2, Table 1) . Although the majority of sites were not installed for geodynamical studies, Hackl *et al.* (2011) show that the stability and performance of the network are well within the requirement for tectonic studies.

Data were processed with Bernese GPS Software, V5.0 (Dach *et al.* 2007) using orbit products from the CODE (Center for Orbit Determination in Europe) Analysis center of the International GNSS Service (IGS) (Dow *et al.* 2009). Double differences of tracking data were analysed in daily batches in ionosphere-free linear combination and phase ambiguities were resolved to integers. Two-hourly troposphere zenith delay and daily gradient parameters were estimated for each station. Station velocities were retrieved by

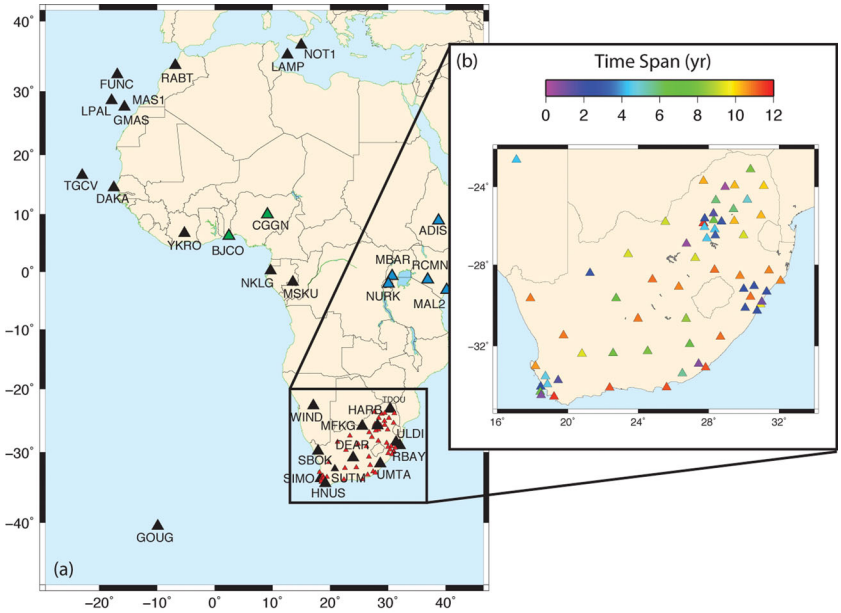

Figure 2. IGS and TrigNet stations processed for this paper. (a) Black triangles: IGS Nubia Plate sites; green triangles sites with short time series; blue triangles Somalia Plate or plate boundary sites; red triangles TrigNet sites. (b) Trignet sites colour coded by the time span of the data processed.

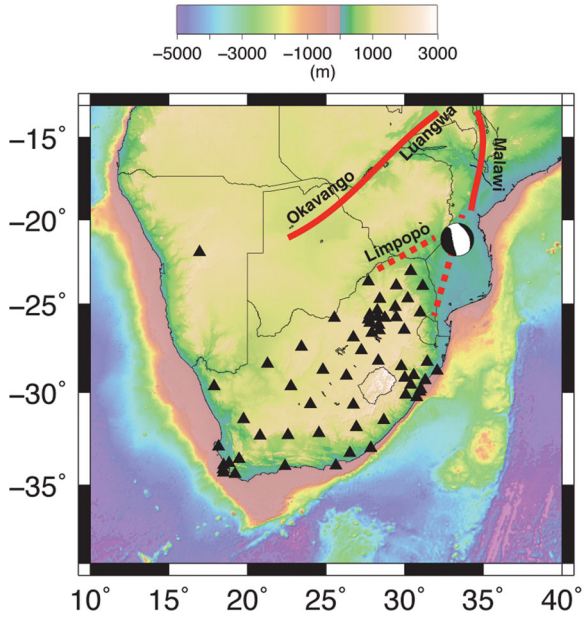

Figure 3. Topographic map of the southern end of the African continent. Black triangles correspond to the TrigNet + WIND GPS stations. Red segments correspond to different branches of the East Africa Rift named as in Fig. 1 (dash possible strain localization areas). Focal Mechanism for the Machaze earthquake from the Global CMT catalog.

combining daily solutions at the normal equation level and corrected for offsets due to known instrument changes. Thirty IGS stations located within and around the Nubia plate were included to realize the geodetic datum. For consistency with the CODE orbits, the network was aligned with the ITRF2005 reference frame (Altamimi *et al.* 2007). Velocity errors were calculated using the Allan Variance of the Rate (AVR) according to Hackl *et al.* (2011) and Hackl (2012) to take into account the presence of time-correlated noise. Table 1 reports station locations, computed velocities and associated uncertainties. A plot of all the time series can be found in the Supporting Information (Fig. S1).

Although the majority of the sites performed extremely well, a few stations had problems and were omitted in our analysis. Stations QTWN and GEOR are a combination of multiple sites loosely connected by survey ties; PRET is installed on an unstable building, SPRT shows an unexplained transient behaviour at the end of 2008 and at the beginning of 2009; and BFTN and TDOU show a very large component of random walk motion probably related to local hydrological effects or monumentation problems. The problem is particularly significant for site BFTN (see Fig. S1 in Supporting Information). Another problematic station is TDOU, but given the importance of the location of this site, we decided to include it in our study. Note that TDOU's associated uncertainties are significantly larger than other sites with similar time length of observation (Table 1). In order to avoid giving too much weight to locations with multiple stations (such as Hartebeesthoek Radio Observatory or the South African Astronomical Observatory), only the stations with the lowest RMS in the velocity linear fit were selected for each site (respectively, HARB and SUTM).

4 TRIGNET VELOCITY FIELD

Assessment of internal plate deformation can be performed with an Euler vector formulation. Given a velocity field describing the motion of a region, an Euler vector that describes the overall motion of geodetic stations can be defined (e.g. Bullard *et al.* 1965; Minster *et al.* 1974). Deviation from rigid plate motion indicates either rigid rotation of an independent block or plate, or internal deformation.

Following the methodology described by Plattner *et al.* (2007), we computed the Euler vector that best describes the observed motion of the TrigNet sites. Of the original 66 TrigNet stations analysed, we eliminated all the stations with less than 1000 d of observation (16 stations), the stations identified as problematic by Hackl *et al.* (2011) (excluded for the initial analysis TDOU), and kept only a single station for each observatory (HARB and SUTM). The Euler vector (pol0) that minimizes the residuals of the remaining 43 stations is given in Table 2. The average rate residual is 0.48 mm yr^{-1} with a reduced χ^2 of 13.4. An analysis of the results shows that removing

Table 1. IGS and TrigNet stations within the study area. In upper case stations utilized for the pol1 analysis. Other TrigNet stations not used in the paper having time series shorter than 1000 d or other problems (see main text) are reported at the end of the table. No velocity is computed for time series shorter than 2.5 yr.

Staz	Lon (deg E)	Lat (deg N)	# of epochs	Start	End	ITRF2005 velocities v_n (mm yr^{-1})	ITRF2005 velocities v_e (mm yr^{-1})
ANTH	26.72	−30.68	2497	2003.04	2011.50	19.20 ± 0.06	16.45 ± 0.04
BENI	28.34	−26.20	1420	2007.05	2011.50	19.07 ± 0.23	16.81 ± 0.48
BETH	28.33	−28.25	3329	2000.56	2011.50	18.64 ± 0.03	16.66 ± 0.02
BWES	22.57	−32.35	1895	2003.78	2011.50	19.68 ± 0.03	16.73 ± 0.05
CALV	19.76	−31.48	3213	2000.67	2011.50	19.71 ± 0.08	17.30 ± 0.05
CTWN	18.47	−33.95	1359	2007.51	2011.50	19.78 ± 0.19	17.03 ± 0.20
DEAR	23.99	−30.67	2894	2000.67	2011.50	19.29 ± 0.02	16.85 ± 0.05
DRBN	30.95	−29.97	2243	2000.59	2010.33	18.04 ± 0.05	16.05 ± 0.02
ELDN	27.83	−33.04	3103	2000.29	2011.50	18.95 ± 0.03	15.55 ± 0.02
EMLO	29.98	−26.50	2781	2002.21	2011.50	17.97 ± 0.07	17.09 ± 0.04
eras	27.70	−23.69	2702	2001.15	2011.50	18.17 ± 0.04	18.32 ± 0.03
GDAL	29.41	−25.16	1182	2005.65	2011.50	18.35 ± 0.09	17.63 ± 0.12
GRHM	26.51	−33.32	1697	2006.00	2011.50	18.76 ± 0.11	15.42 ± 0.26
grnt	24.53	−32.25	2017	2003.50	2011.50	19.69 ± 0.04	17.73 ± 0.03
HARB	27.71	−25.89	3627	2000.61	2011.50	18.94 ± 0.02	17.80 ± 0.05
HNUS	19.22	−34.42	3024	2000.00	2011.50	19.72 ± 0.05	16.61 ± 0.05
hrao	27.69	−25.89	3859	2000.00	2011.50	18.35 ± 0.04	17.71 ± 0.03
KLEY	24.81	−28.74	2688	2000.58	2011.50	18.98 ± 0.09	17.37 ± 0.09
KMAN	23.43	−27.46	2799	2002.29	2011.50	19.03 ± 0.08	18.05 ± 0.03
krug	27.77	−26.08	1413	2007.06	2011.50	19.39 ± 0.23	16.71 ± 0.91
KSTD	27.24	−27.66	2339	2002.30	2011.50	18.61 ± 0.05	17.15 ± 0.07
LGBN	18.16	−32.97	2931	2001.00	2011.50	19.70 ± 0.09	17.48 ± 0.04
LSMH	29.78	−28.56	2757	2000.58	2011.29	18.59 ± 0.03	16.67 ± 0.02
MALM	18.73	−33.46	1497	2006.90	2011.50	19.85 ± 0.30	16.72 ± 0.23
MBRG	29.45	−25.77	2910	2001.21	2011.50	18.92 ± 0.06	17.60 ± 0.06
MBRY	18.47	−33.95	1070	2005.17	2007.48	19.78 ± 0.12	17.03 ± 0.13
mfkg	25.54	−25.81	2231	2002.33	2011.50	20.11 ± 0.11	18.62 ± 0.17
NSPT	30.98	−25.48	2797	2001.21	2011.50	18.19 ± 0.20	17.14 ± 0.07
NYLS	28.41	−24.70	1739	2005.65	2011.50	18.55 ± 0.08	18.03 ± 0.08
pbwa	31.13	−23.95	2733	2001.44	2011.50	17.90 ± 0.06	17.48 ± 0.04
PELB	25.61	−33.98	2416	2000.28	2011.50	19.08 ± 0.31	15.65 ± 0.09
PMBG	30.38	−29.60	2180	2000.58	2011.50	18.21 ± 0.03	15.69 ± 0.02
PSKA	22.75	−29.67	2236	2004.59	2011.50	19.34 ± 0.11	17.50 ± 0.06
PTBG	29.47	−23.92	2589	2001.22	2011.50	18.63 ± 0.06	17.50 ± 0.12
RBAY	32.08	−28.80	2156	2000.76	2011.50	18.15 ± 0.03	16.07 ± 0.07
SBOK	17.88	−29.67	3311	2000.64	2011.50	19.57 ± 0.05	18.08 ± 0.06
SIMO	18.44	−34.19	1429	2001.60	2009.01	19.82 ± 0.09	16.51 ± 0.05
STBS	18.84	−33.84	1506	2006.92	2011.50	20.02 ± 0.19	16.91 ± 0.23
suth	20.81	−32.38	3741	2000.00	2011.50	19.53 ± 0.06	16.86 ± 0.05
SUTM	20.81	−32.38	3196	2002.19	2011.50	19.51 ± 0.06	17.04 ± 0.03
tdou	30.38	−23.08	2243	2003.46	2011.50	16.95 ± 0.27	18.13 ± 0.25
ULDI	31.42	−28.29	3073	2000.71	2011.50	18.25 ± 0.06	16.46 ± 0.03
umta	28.67	−31.55	3066	2000.56	2011.50	18.43 ± 0.03	16.02 ± 0.02
UPTN	21.26	−28.41	1224	2007.84	2011.50	19.38 ± 0.11	18.26 ± 0.12
VERG	27.90	−26.66	1467	2007.07	2011.50	18.76 ± 0.12	17.19 ± 0.13
WIND	17.09	−22.57	1458	2007.12	2011.50	19.74 ± 0.11	19.98 ± 0.13
			Other TrigNet stations not used in this paper				
bftn	26.30	−29.10	2684	2000.50	2011.27	17.29 ± 0.47	17.99 ± 1.73
biso	27.43	−32.86	178	2010.77	2011.50		
brit	27.78	−25.64	702	2008.86	2011.50		
brnk	28.73	−25.80	961	2008.62	2011.50	18.93 ± 1.28	17.48 ± 0.77
cptn	18.49	−34.35	210	2010.69	2011.50		
drba	31.02	−29.85	269	2010.47	2011.50		
geor	22.38	−34.00	2530	2000.26	2011.50	19.46 ± 0.07	16.33 ± 0.05
grey	30.58	−29.07	751	2009.09	2011.50		
heid	28.37	−26.51	960	2008.45	2011.50	18.37 ± 0.91	17.82 ± 0.89
ixop	30.07	−30.15	828	2008.84	2011.50		
mriv	29.99	−29.21	750	2009.17	2011.50		
okny	26.74	−26.93	119	2010.95	2011.50		

Table 1. (*Continued.*)

Staz	Lon (deg E)	Lat (deg N)	# of epochs	Start	End	ITRF2005 velocities v_n (mm yr^{-1})	v_e (mm yr^{-1})
potg	28.93	−24.01	34	2011.19	2011.50		
pret	28.28	−25.73	2376	2004.02	2011.50	17.23 ± 0.09	17.76 ± 0.09
qtwn	26.92	−31.91	2091	2004.62	2011.50	19.12 ± 0.21	15.50 ± 0.33
scot	30.75	−30.29	760	2009.17	2011.50		
sprt	30.19	−24.67	1625	2006.57	2011.50	19.26 ± 0.38	19.21 ± 0.48
stan	31.29	−29.34	834	2008.89	2011.50		
temb	28.27	−25.38	462	2009.94	2011.50		
upta	21.26	−28.41	720	2004.92	2007.77		
worc	19.45	−33.64	472	2009.94	2011.50		

the sites ERAS, GRNT, KRUG, MFKG, PBWA, TDOU and UMTA significantly improves the solution with a new average residual of 0.24 mm yr^{-1} and reduced χ^2 of 1.02 (pol1, Table 2, Fig. 4). Although the propagation of the East African Rift could be one of the explanations for the higher Northeastern residuals, anthropogenic effects could also play an important role. The sites GRNT, UMTA (one of the longest time series) and BWES are emblematic from this point of view. Situated essentially in the middle of the country and surrounded by sites with much smaller residuals, they lie very close (within 1 km) to artificial lakes controlled by dams (Nqweba and Mtata, respectively, for GRNT and UMTA, and Leeu-Gamka Dam for BWES). It is possible that these sites are affected by the loading/unloading of the lakes, a hypothesis supported by the fact that the residuals are pointing radially with respect to the centre of each lake. For example, two years ago the region around BWES was affected by a severe drought that left the Leeu-Gamka lake completely dry. A Boussinesq's approximation of the elastic deformation (Saada 1974) due to the complete unloading of the 42×10^6 m^3 reservoir leads to up to 2 cm displacement at the location of BWES. Unfortunately, the lack of publicly available water level data does not allow for detailed modelling of the loading effects.

The residual velocity field for 34 of the 36 stations in the pol1 solution is within the 95 per cent confidence ellipse (Table S1). Still, it is interesting that all the stations in the northeast region (in red in Fig. 4) are systematically pointing to the south–west, while the sites in the Cape Town area (in blue in Fig. 4) are systematically pointing to the northeast. The direction of the residuals for the northeastern sites is compatible with an influence of the Mw7.0 2006 February 22 Machaze earthquake in Mozambique (21.26S, 33.48E) (Fenton & Bommer 2006), although the distance of the event from the network is significant (∼300 km from TDOU). To test this possibility as well as the influence of spatially long-term time-correlated signal on the velocity field, we truncate our analysis at different times (2006, 2007, 2008 and 2009) calculating a new Euler vector and residuals for each analysis. As expected, residuals and uncertainties for the shorter time series increase significantly and all the residuals are compatible with the corresponding 95 per cent confidence interval for all the analysis. The systematic spatial correlation of the sites in the northeast is persistent in time series truncated at 2008 or later, but disappears when the time series are truncated at 2006 or 2007 (Fig. S3). A systematic analysis of the effect of the Mozambique earthquake is beyond the aim of this paper but these results suggest that despite the distance to the epicentre, observed site velocities for the northeast stations may be influenced by such an event. Indeed, while a co-post-seismic displacement is not immediately visible in the time series, an analysis of the 'colour' of the noise content of the time series indicates that the northeast sites tend to be closer to random walk than the rest of the network, a possible sign of the influence of a transient event (Hackl 2012). On the other hand, the systematic northwest-directed residuals in the Cape Town area are present in all the analysis, suggesting that it is not related to biases introduced by long-time-correlated signals (e.g. seasonal effects).

To test the stability and the uncertainties associated with the location of the Euler vector pol1, we used a jackknife analysis, where the best fit Euler vector was recomputed after removing 1, 2 or 3 sites from the 36 'stable TrigNet' stations. Of the 44 137 computed vectors, 42 135 lie within the 95 per cent error ellipse defined following the method of Ward (1990). The jackknife solutions show a slight improvement when the sites in the northeast or the sites around the Cape Town regions are removed. Still, the reduction of the reduced χ^2 is not statistically significant, using the *F*-test (Stein & Gordon 1984). Pol5 (Table 2) corresponds to the extreme case where only 14 stations from regions with strain rate lower than 0.5 nanostrain yr^{-1} are used (reduced $\chi^2 = 0.7$, average residual 0.15 mm yr^{-1}). Even in this case, the difference between the pol1 and pol5 is not statistically significant.

As a final step, we validated the AVR uncertainties by looking at the statistical consistency of the velocity field described by the 19 sites within the central part of the network (considered to be the most stable region), observing how many sites have residuals within 95 per cent, 66 per cent, and 50 per cent confidence ellipses (similar to McClusky *et al.* 2000; Davis *et al.* 2003; McCafrey *et al.* 2007). While only two sites are barely outside the 95 per cent confidence interval, seven fall outside the 66 per cent confidence ellipse, and 10 residuals are larger than the 50 per cent error ellipse, indicating that our estimation of uncertainties is statistically consistent with the Eulerian description of the 'stable' TrigNet velocity field. Fig. S4 in the Supporting Information summarizes these results.

5 TRIGNET INTERNAL STRAIN

As a further step to evaluate the rigidity of the TrigNet region, we performed an analysis of the intra-network strain rates. Diffuse plate boundaries within plate interiors such as the Basin and Ranges in North America have strain rates of the order of tens of nanostrains per year (1 nanostrain yr^{-1} is equivalent to 3.2×10^{-17} s^{-1})(e.g. Bennett *et al.* 2003; Malservisi *et al.* 2003; Hackl *et al.* 2009; Plattner *et al.* 2010). For comparison, it is typically assumed that rigid plate behaviour is indicated by strain rates of the order of a few nanostrain per year or lower (Gordon 1998).

For each pair of stations with at least 1000 d of common observations, we computed the daily ellipsoidal distance (Vincenty 1975) from the observed latitude and longitude. These time series were interpolated with a linear fit and the strain rate computed, dividing the rate of change of the distance (the slope from the fit) by the

Table 2. Euler vectors (ITRF2005) that minimize the residuals of TrigNet stations. In bold our preferred solution (see text for description).

Pole	No. Stat.	$\frac{\chi^2}{DOF}$	Av. Resid. (mm yr^{-1})	Ω_{Lat} (°N)	Ω_{Lon} (°E)	σ_{max} Max Axis	σ_{min} Min Axis	φ Azim.	Ω (deg Myr^{-1})
pol0	43	13.4	0.48	49.22	−79.42	1.99	0.15	−81.2	0.272 ± 0.004
pol1	**36**	**1.02**	**0.24**	**49.71**	**−82.39**	**0.64**	**0.08**	**−83.5**	**0.275 ± 0.002**
pol5	14	0.70	0.15	49.53	−80.31	1.45	0.10	−78.5	0.271 ± 0.003
	Ω_x†	Ω_y†	Ω_z†	Σ_{xx}‡	Σ_{yy}‡	Σ_{zz}‡	Σ_{xy}‡	Σ_{xz}‡	Σ_{yz}‡
pol0	0.5697	−3.0496	3.5966	0.01103	0.00312	0.00462	0.00579	−0.00706	−0.00373
pol1	**0.4112**	**−3.0789**	**3.6644**	**0.00123**	**0.00035**	**0.00052**	**0.00064**	**−0.00079**	**−0.00042**
pol5	0.5170	−3.0273	3.5998	0.00590	0.00115	0.00240	0.00255	−0.00375	−0.00163

† Cartesian components Euler vector 10^{-3}(rad Myr^{-1}).
‡Covariance Matrix Euler vector in cartesian components 10^{-6}(rad Myr^{-1})^2.

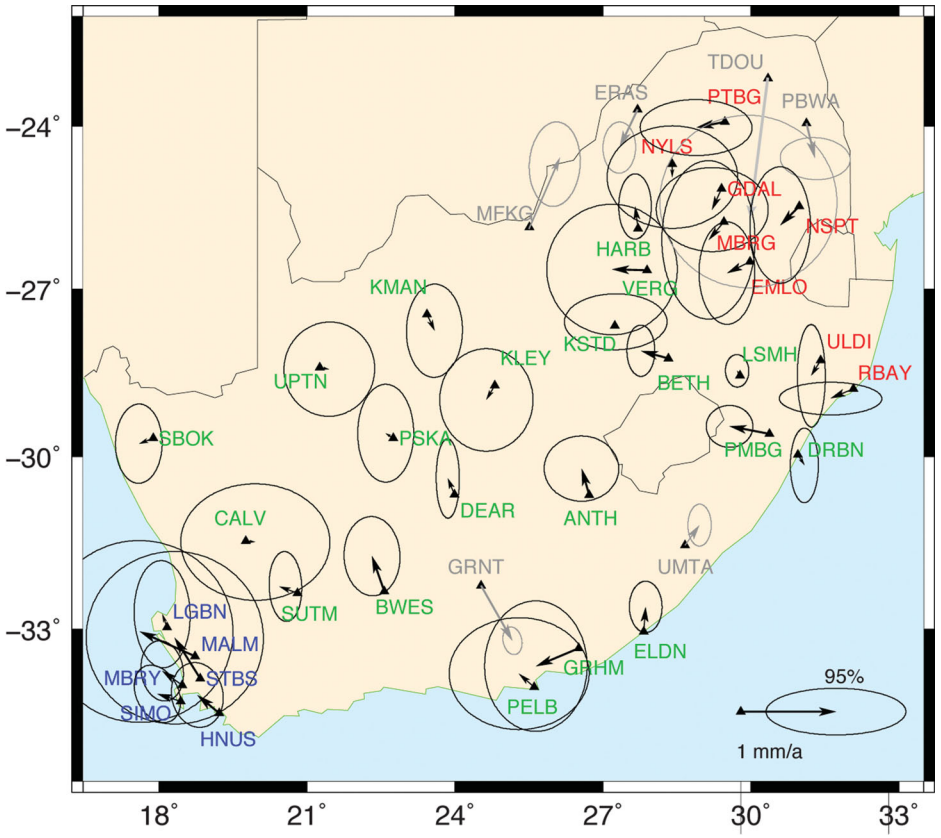

Figure 4. Velocity field with respect to the motion described by the Euler vector that minimizes the residuals for the TrigNet data (pol1 in Table 2). All the sites except for the ones marked in grey were utilized for the computation of the Euler vector. Blue and red colours indicate sites with velocities in coherent azimuth directions. Respectively, in the Cape Town and North East regions (see text for explanation). Mean rate of all vector is 0.24 mm yr^{-1}.

initial length of the geodesic connecting the two points. Uncertainties were computed analysing the obtained time series with the AVR (Hackl *et al.* 2011; Hackl 2012) thus including coloured noises. The importance of including coloured noise in the uncertainties estimation is illustrated by the baseline DEAR-BFTN. While DEAR is one of the most stable sites of the network, site BFTN is strongly affected by time-correlated noise. The resulting time series of the change of geodesic length is thus affected by the noise of BFTN. The computed strain rate along the arc between the two stations is 18 nanostrain yr^{-1}. When the formal error is computed assuming purely Gaussian (white) noise, we get a value of 1 nanostrain yr^{-1}. The analysis with AVR shows the presence of a very large component of random walk and the resulting uncertainty is of the order of 20 nanostrain yr^{-1}. A strain rate that appears significant (18 ± 1 nanostrain yr^{-1}) when uncertainties are evaluated without accounting for time-correlated noise is thus reduced to a noisy data point (18 ± 20 nanostrain yr^{-1}) once the presence of random walk noise is taken into account. This large uncertainty is why we decided not to use station BFTN.

In order to better describe the pattern of strain rate, we chose to limit our discussion to a subset of ellipsoidal arcs selected as the connections in a 2-D Delauany triangulation (Schewchuk 1996). Use of the full data set would result in much larger complexity but would not alter our conclusions. Fig. 5(a) shows the strain rate computed by the change of distance between two connected stations. The lines are colour-coded according to the average magnitude of

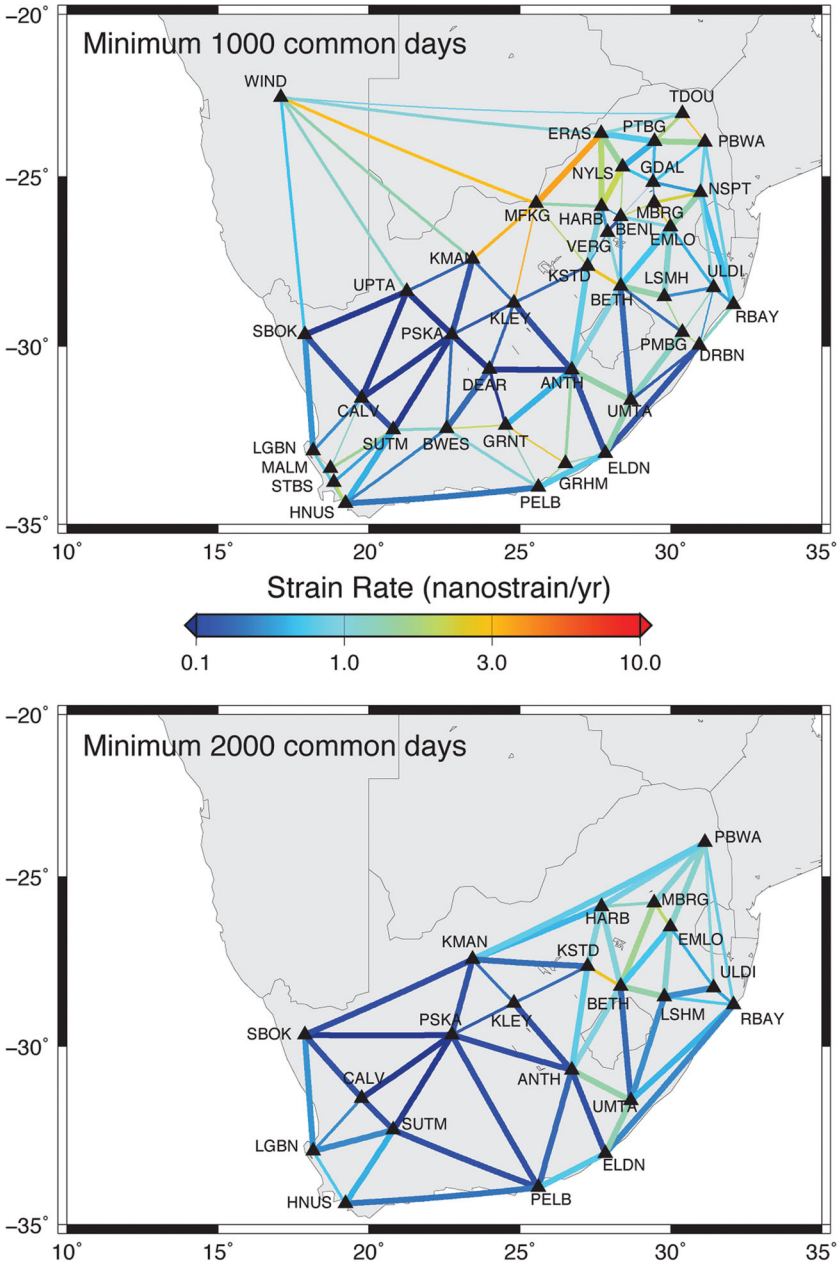

Figure 5. TrigNet strain rate map. Relative changes of length for the geodesic between TrigNet stations connected by a 2-D Delauany triangulation. Geodesics of the top figure connect sites with at least 1000 common days, while the lower figures correspond to at least 2000 common days. Note that the strain rate is smaller than 3 nanostrain yr^{-1} in the full network, indicating essential rigidity of the system. Line thickness indicates the uncertainties associated with the measurement (thicker lines correspond to lower uncertainties). The presence of a region with lower strain rate in the western part of the network also for time series longer than 2000 d and the homogeneous distribution of such baselines suggest that the slightly higher strain rate in the Cape Town region and the eastern part of the network are not due to temporally correlated signals.

the strain rate along the connecting geodesics (in nanostrain per year), while the thickness represents the uncertainty associated with each line (thick lines correspond to lower uncertainties). A look at the colour scale immediately indicates that the maximum observed strain rate has values smaller than a few nanostrain per year, well within typical values for rigid plate interior. The average strain rate for the full network is 0.97 ± 0.7 nanostrain yr^{-1}.

Although the strain rate over the full network is consistent with plate rigidity, Fig. 5(a) delineates an interesting geographical pattern: strain rates in the western part of the network are smaller than strain rates in the eastern part. This division does not correlate with the boundaries of the cratonic root (Fig. 1) as defined by seismic tomography (e.g. Begg *et al.* 2009) nor is it influenced by the distribution of stations with different time series length (Fig. 5). Instead, it is correlated with the population density [http://www.statssa.gov.za/census01/html/default.asp (last accessed 21 December 2012)], crop growth (e.g. Estes *et al.* 2011) and mining concentration. This suggests an anthropogenic source in the eastern region where population is concentrated, or possible higher noise levels due to higher humidity in the air affecting troposphere parameter estimation or, in the soil causing multipath (e.g. Larson *et al.* 2008). Still, it is worthy to note that a similar geographical

Table 3. Difference between previously published poles in cartesian coordinates (Table 3) and pol1.

Pole	$\delta\Omega_x(10^{-3}$ rad Myr$^{-1})$	$\delta\Omega_y(10^{-3}$ rad Myr$^{-1})$	$\delta\Omega_z(10^{-3}$ rad Myr$^{-1})$
S08	-0.03 ± 0.23	-0.45 ± 0.09	0.34 ± 0.06
A07	0.02 ± 0.11	-0.08 ± 0.05	0.07 ± 0.05
N06	-0.01 ± 0.04	-0.37 ± 0.03	0.27 ± 0.03
F04	0.06 ± 0.09	-0.32 ± 0.05	0.16 ± 0.05
PB04	0.01 ± 0.09	0.04 ± 0.14	-0.30 ± 0.12
DEOS2k	-0.02 ± 0.19	-0.24 ± 0.10	0.13 ± 0.10
REVEL	-0.05 ± 0.09	-0.42 ± 0.06	0.17 ± 0.07
pol5	-0.11 ± 0.08	-0.05 ± 0.04	0.06 ± 0.05

division is suggested by the propagation of the Nubia/Somalia complex plate boundary southward into the South African region where the Nubia/Somalia relative displacement could be accommodated in a broad deformation zone (Hartnady 1990, 2002; Stamps *et al.* 2008).

Larger than average strain rate is also observed around the Cape Town region (sites HNUS, LGBN, MALM, SIMO and STBS). While it is likely that anthropogenic deformation is significant here, the region has significant (magnitude ∼6) historical seismicity (Maasha & Molnar 1972; Midzi *et al.* 1999; Hartnady 2002; Brandt *et al.* 2005) probably associated with faults within the old deformation belt. Models of the postseismic deformation due to the Mw6.3 Ceres earthquake of 1969 (Maasha & Molnar 1972) indicate that it is not responsible for the anomalous strain rate of the region.

As already identified in the velocity residuals analysis, the largest deformation within the TrigNet network is observed around the new IGS site of Mafikeng (MFKG), most likely related to localized deformation (also probably induced by human activities).

To the north, the geodesics connecting the IGS site WIND with the northern stations of TrigNet show a higher than average strain rate, increasing from west to east, compatible with the propagation of the South Western Branch of the East Africa Rift along the Okavango–Luangwa or possibly the Limpopo basins. Unfortunately, the lack of stations north of the border with time series long enough to provide significant results does not allow us to quantify or localize such deformation.

While we do not find significant correlation between computed strain rate and baseline length, geodesics with longer time series tend to present lower strain rates. This suggests that our results define an upper limit to plate rigidity. The lower strain rate associated with longer observations, where long temporal correlation and seasonal effects are averaged out, (Figs 5a and b) also suggests the importance of noise analysis in low strain rate regions.

6 NUBIA AND TRIGNET NETWORK's EULER VECTOR

Given the limited available data, determination of a GPS-based Euler vector for Nubia plate is problematic. Compared with other plates of similar size, previously published Euler vectors present relatively larger uncertainties and, in general, do not overlap within 95 per cent confidence interval (Tables S2 and S3).

The Euler vector defined by the 38 'stable TrigNet' sites (pol1) overlaps within uncertainties with the result from Altamimi *et al.* (2007) but has significantly larger magnitude than all of the other published models (Tables S2 and S3). Since the Euler vectors of Table S3 describe the rigid block motion of the Nubia plate with respect to ITRF2005 while pol1 describes the motion of the TrigNet region with respect to the same reference, the difference between the two vectors (Table 3) describes the relative motion between the South African region and the Nubia plate. The rigid body rotation described by the difference vector points southwest with magnitudes ranging from 0.6 mm yr^{-1} ((Altamimi *et al.* 2007)—pol1) to 2.1 mm yr^{-1} (Nocquet *et al.* (2006)—pol1) (Fig. S5). This motion is compatible with a clockwise rotation of South Africa with respect to the Nubia plate, as would be expected by the propagation of the East African Rift along the Okavango Luangwa region. In reality, the assumption that the difference vectors represent the relative motion of Nubia and South Africa is not completely correct because all the computed Euler vectors in Table S3 include sites within South Africa. A cleaner approach certainly would be to estimate the Nubia-TrigNet Euler vector directly from the site on the Nubia plate excluding the South African sites. Unfortunately, at the state (June 2011), data limitation precludes a more in-depth study.

Residuals of IGS sites within the Nubia plate with at least 3 yr of data also suggest relative motion between the TrigNet network and the rest of the plate (Fig. 6, Table S4). Although the average residual is close to or within the 95 per cent confidence interval, all

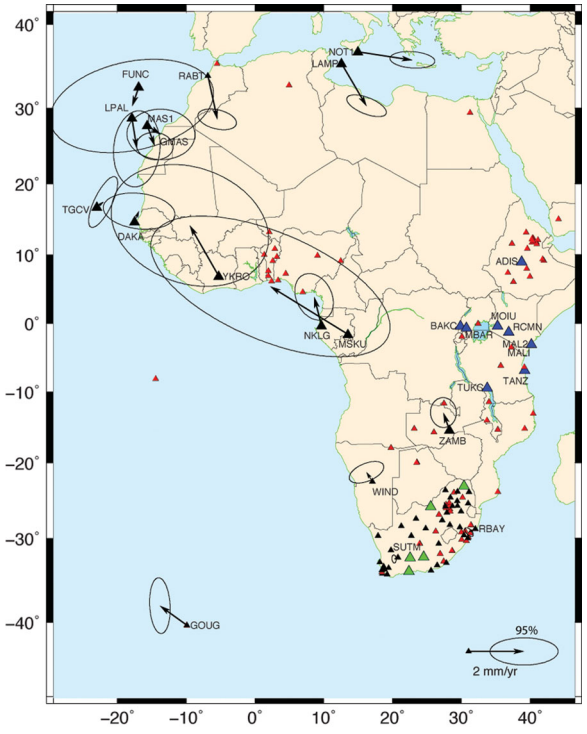

Figure 6. Nubia Plate IGS site velocities with respect to the reference frame defined by pol1 (black arrows and triangles). Blue triangles correspond to IGS sites not within stable Nubia plate, red triangles to new sites processed in this work but with time series too short to give significant velocities or new AFREF/Africa Array sites only recently publicly available.

sites south of 20°N point to the north. In particular, the residuals for GOUG, WIND, and ZAMB indicate some northward motion with respect to South Africa. Unfortunately, the sites in central Africa that could confirm this trend have discontinuous time series and hence very large uncertainties, and are not sufficiently reliable to constrain the rigidity of the plate. To the north, sites in the Canary Islands and in Morocco have significant residuals pointing to the south, compatible with a deformation zone due to the collision of the Nubia and Eurasia plates.

7 DISCUSSION AND CONCLUSIONS

The analysis of the TrigNet data set indicates that the South African region is indeed rigid within the measurement uncertainties, and present strain rates of the order of 1 nanostrain yr^{-1}. Although typical for strain rates normally associated with stable plate interiors, the east part of South Africa and the Cape Town regions exhibit a slightly higher strain rate. While it is possible that these 'higher' strain rates are related to the tectonic activity indicated by the presence of historical seismicity in the Cape Town area, a poorly defined boundary between the Nubia and the Somalia plates in the Mozambique Belt region, or the 2006 Machaze earthquake, it is likely that a significant part of the observed strain rate is induced by human activity (related to agricultural and extractive industries) or it is related to increased noise due to natural effects such as atmospheric water vapour. Analysis of the TrigNet data indicates that unless we are able to separate the contribution of different kinds of noise present in the GPS time series, it will be very difficult to estimate small deformations due to possible tectonic processes within stable regions.

Similarly, it is difficult to extend the analysis of GPS velocity field within cratonic regions to a seismic hazard study. Seismicity in low deformation regions like cratons presents a complex spatial and temporal distribution (e.g. Li *et al.* 2009; Liu *et al.* 2011). Intraplate earthquakes appear to cluster both temporally and spatially on a complex system of ancient faults or crustal weaknesses with long dormancy periods (Calais *et al.* 2005, 2011; Li *et al.* 2009). South Africa is not an exception from this point of view with historical and instrumental significant seismicity ($M > 5$) concentrated in few well-localized clusters (Midzi *et al.* 1999; Davies & Kijko 2003; Brandt *et al.* 2005; Singh & Hattingh 2009; Singh *et al.* 2009, 2011). It is interesting to note that while two of the clusters (Cape Town and Ceres) lie in the higher strain rate regions, the 1976 intensity VII event of Kaffiefontain earthquake (between KLEY and ANTH) or the currently active swarm of Grootvloer (between UPTA and SBOK) are not appearing in our analysis.

While the South African region behaves rigidly, the question of how much deformation is accommodated within the Nubia plate is still open. The difference between the magnitudes of the Euler vectors computed for the full Nubia plate and the one from TrigNet suggest the possibility of internal deformation of the order of 0.5–2 mm yr^{-1}. Still, it is very likely that the published Euler poles of the full plate are biased by the use of sites in South Africa and possibly by sites within the northern deformational region. Unfortunately, the paucity of sites in the stable region of Nubia and the limited stability of some IGS sites such as TGCV, YKRO or MSKU does not allow for a better constraint. Significant residuals pointing to the north for the sites WIND, ZAMB, GOUG and NKLG with respect to a stable TrigNet suggest the possibility of Nubia deformation of the order of 0.5–1.5 mm yr^{-1}. From a geological point of view, the major candidate for this internal deformation is the southwest propagation of the East African Rift into the Okavango–Luangwa or possibly Limpopo basins; still the large uncertainties and the sparse network do not allow for any constraints on the localization of the deformation.

Regarding the current published Euler poles for the Nubia plate, it is important to note that the current distribution of GPS instruments is non-ideal and it is possible that the current description of the motion of Nubia from geodetic data is biased by some degree of internal deformation. The development of a continental network within the framework of AFREF (a UN sponsored initiative to create an unified reference frame for Africa), the collocation of GPS systems with the AfricaArray seismic network, and different international projects are increasing the amount of publicly available data in Africa. These data will lead to significant improvement in the next few years.

ACKNOWLEDGMENTS

We wish to thank T.H. Dixon, C. Ebinger, R. King, A. McGarr, V. Midzi, R. Durrheim, C. Hartnady and V. Dennis for the interesting discussions and suggestions that significantly improved the paper. The authors would like to thank the operators of the CGPS sites used in this study. A particular thank to TrigNet for the availability of the data and for their support. All figures have been produced using Generic Mapping Tools (Wessel & Smith 1998).

REFERENCES

Altamimi, Z., Collilieux, X., Legrand, J., Garayt, B. & Boucher, C., 2007. ITRF2005: a new release of the International Terrestrial Reference Frame based on time series of station positions and Earth orientation, *J. geophys. Res.,* **112,** B09401, doi:10.1029/2007JB004949.

Andreoli, M., Doucoure, M., Van Bever Donker, J., Brandt, D. & Andersen, N., 1996. Neotectonics of Southern Africa: a review, *Afr. Geosci. Rev.,* **3,** 1–16.

Begg, G. *et al.*, 2009. The lithospheric architecture of Africa: seismic tomography, mantle petrology, and tectonic evolution, *Geosphere,* **5,** 23–50, doi:10.1130/GES00179.1.

Behn, M., Conrad, C. & Silver, P., 2004. Detection of upper mantle flow associated with the african superplume, *Earth planet. Sci. Lett.,* **224,** 259–274.

Bennett, R., Wernicke, B., Niemi, N., Friedrich, A. & Davis, J., 2003. Contemporary strain rates in the northern Basin and Range province from GPS data, *Tectonics,* **22,** doi:10.1029/2001TC001355.

Brandt, M.B.C., Bejaichund, B., Kgaswane, E.M., Hattingh, E. & Roblin, D.L., 2005. *Seismic History of Southern Africa,* Council for Geoscience, Pretoria, South Africa.

Bullard, E., Everett, J.E. & Smith, A., 1965. Fit of continents around Atlantic, in *A Symposium in Continental Drift,* Vol. 258, pp. 41–75, eds Blackett, P., Bullard, E. & Runcorn, S., Roy. Soc. London, Phyl. Trans. Ser. A.

Burke, K., 1996. The African plate, *S. Afr. J. Geol.,* **99,** 339–410.

Calais, E., Ebinger, C., Hartnady, C. & Nocquet, J., 2006. Kinematics of the East African rift from GPS and earthquake slip vector data, in *The Afar Volcanic Province Within the East African Rift System,* Vol. 259, pp. 9–22, eds Yirgu, G., Ebinger, C. & Maguire, P., Special Publications: London, Geological Society.

Calais, E., Freed, A., Van Arsdale, R. & Stein, S., 2011. Triggering the New Madrid seismicity by late-Pleistocene erosion, *Nature,* **466,** doi:10.1038/nature09558.

Calais, E., Mattioli, G., DeMets, C., Nocquet, J.-M., Stein, S., Newman, A. & Rydelek, P., 2005. Tectonic strain in plate interiors? *Nature,* **438,** doi:10.1038/nature04428.

Dach, R., Hugentobler, U., Fridez, P. & Meindl, M., 2007. *Bernese GPS Software Version 5.0. User Manual,* Bern, Switzerland.

Dalziel, I., Mosher, S. & Gahagan, L., 2000. Laurentia-Kalahari collision and the assembly of Rodinia, *J. Geol.,* **108,** 499–513.

Davis, J., Bennett, R. & Wernicke, B., 2003. Assesment of GPS velocity accuracy for the Basin and Range Geodetic Network (BARGEN), *Geophys. Res. Lett.,* **30,** 1441, doi:10.1029/2003GL016961.

Davies, N. & Kijko, A., 2003. Seismic risk assessment with application to the South African insurance industry, *S. Afr. Actuarial J.,* **3,** 1–28.

DeMets, C., Gordon, R., Argus, D. & Stain, S., 1990. Current plate motion, *Geophys. J. Int.,* **101,** 425–478.

DeWit, M., Stankiewicz, J. & Reeves, C., 2000. Restoring Pan-African-Breasiliano connections: more Gondwana control, less Trans-Atlantic corruption, in *West Gondwana: Pre-Cenozoic Correlations Across the South Atlantic Region,* Vol. 294, pp. 399–412, eds, Pankhurst, R., Trouw, R., Brito Neves, B. & De Wit, M., Geological Society, London, Special Publications.

Dixon, T., 1991. An introduction to the global positioning system and some geological applications, *Rev. Geophys.,* **29,** 249–276.

Dixon, T., Mao, A. & Stein, S., 1996. How rigid is the stable interior of the North American plate?, *Geophys. Res. Lett.,* **23,** 3035–3038.

Dow, J., Neilan, R. & Rizos, C., 2009. The International GNSS Service in a changing landscape of Global Navigation Satellite System, *J. Geod.,* **83,** 191–198, doi:10.1007/s00190-008-0300-3.

Drewes, H., 1982. A geodetic approach for the recovery of global kinematic plate parameters, *Bull. Geod.,* **56,** 70–79.

Eagles, G., 2007. New angles on South Atlantic opening, *Geophys. J. Int.,* **168,** 353–361.

Ebinger, C., 1989. Tectonic development of the western branch of the East African Rift System, *Geol. Soc. Am. Bull.,* **101,** 885–903.

Ebinger, C., Bechtel, T., Forsyth, D. & Bowin, C., 1989. Effective elastic plate thickness beneath the East African and Afar Plateaus and dynamic compensation of the uplifts, *J. geophys. Res.,* **94,** 2883–2901.

Ebinger, C. & Sleep, N., 1998. Cenozoic magmatism throughout East Africa resulting from the impact of a single plume, *Nature,* **395,** 788–791.

Erlank, A., Marsh, J., Duncan, A., Miller, R., Hawesworth, C., Betton, P. & Rex, D., 1984. Geochemistry and petrogenesis of the Etendeka volcanic rocks from SWA/Namibia, *Spec. Publ. Geol. Soc. S. Africa,* **13,** 195–245.

Estes, L., Bradley, B., Oppenheimer, M., Wilcove, D., Beukes, H., Schulze, R. & Tadross, M., 2011. South African maize production scenarios for 2055 using a combined empirical and process-based model approach, *Paper presented at AGU 2011 Fall Meeing, EOS Trans.,* pp. GC13A–0951.

Fairhead, J. & Henderson, N., 1977. The seismicity of Southern Africa and incipient rifting, *Tectonophysics,* **41,** 19–26.

Fenton, C. & Bommer, J., 2006. The Mw 7 Machaze, Mozambique, earthquake of 23 February 2006, *Seism. Res. Lett.,* **77,** 426–439, doi:10.1785/gssrl.77.4.426.

Fernandes, R., Ambrosius, B., Noomen, R., Bastos, L., Wortel, M., Spakman, W. & Govers, R., 2003. The relative motion between Africa and Eurasia as derived from itrf2000 and gps data, *Geophys. Res. Lett.,* **30,** 1828, doi:10.1029/2003GL017089.

Fernandes, R., Ambrosius, B., Noomen, R., Bastos, L., Combrinck, L., Miranda, J. & Spakman, W., 2004. Angular velocities of Nubia and Somalia from continuous gps data: implications on present-day relative kinematics, *Earth planet. Sci. Lett.,* **222,** 197–208, doi:10.1016/j.epsl.2004.02.008.

Forte, A., Quere, S., Moucha, R., Simmons, N.A., Grand, S., Mitrovica, J. & Rowley, D., 2010. Joint seismic-geodynamic-mineral physical modeling of African geodynamics: a reconciliation of deep mantle convection with surface geophysical constraints, *Earth planet. Sci. Lett.,* **295,** 329–341.

Gordon, R., 1998. The plate tectonic approximation: plate non-rigidity, diffuse plate boundaries, and global plate reconstruction, *Ann. Rev. Earth planet. Sci.,* **26,** 615–642.

Graham, G. & Brandt, M., 2000. *Seismicity of Sub-Saharan Africa,* Pretoria, South Africa.

Gumbricht, T., McCarthy, T. & Merry, C., 2001. The topography of the Okavango Delta, Botswana, and its tectonic and sedimentological implications, *S. Afr. J. Geol.,* **104,** 243–264.

Gurnis, M., Mitrovica, J., Ritsema, J. & van Heijst, H., 2000. Constraining mantle density structure using geological evidence of surface uplift rates: the case of the African superplume, *Geochem. Geophys. Geosyst.,* **3,** doi:10.1029/1999GC000035.

Hackl, M., 2012. GPS analysis: strain, transients, and colored noise, *PhD thesis,* Ludwig-Maximilians University, Munich, Germany.

Hackl, M., Malservisi, R. & Wdowinski, S., 2009. Strain patterns from dense GPS networks, *Nat. Hazards Earth Syst. Sci.,* **9,** 1177–1187.

Hackl, M., Malservisi, R., Hugentobler, U. & Wonnacott, R., 2011. Estimation of velocity uncertainties from GPS time series: examples from the analysis of the South African TrigNet network, *J. geophys. Res.,* **116,** B11404, doi:10.1029/2010JB008142.

Hartnady, C., 1990. Seismicity and plate boundary evolution in Southeastern Africa, *S. Afr. J. Geol.,* **93,** 473–484.

Hartnady, C., 2002. Earthquake hazard in Africa: perspectives on the Nubia-Somalia boundary, *S. Afr. J. Sci.,* **98,** 425–428.

Hlatywayo, D., 1997. Seismic hazard in central Southern Africa, *Geophys. J. Int.,* **130,** 737–745.

International Seismological Centre, 2010. *On-Line Bulletin,* International Seismological Centre, Thatcham, United Kingdom, http://www.isc.ac.uk, (last accessed 21 December 2012).

Kinabo, B., Atekwana, E., Hogan, J., Modisi, M., Wheaton, D. & Kampunzu, A., 2007. Early structural development of the Okavango Rift Zone, NW Botswana, *J. Afr. Earth Sci.,* **48,** 125–136.

Kinabo, B., Hogan, J., Atekwana, E., Abdel Salam, M. & Modisi, M., 2008. Fault growth and propagation during incipient continental rifting: inside from a combined aeromagnetic and Shuttle Radar Topography Mission digital elevation model investigation of the Okavango Rift Zone, northwest Botswana, *Tectonics,* **27,** doi:10.1029/2007TC002154.

Kröner, A. & Cordani, U., 2003. African, southern Indian, and South American cratons were not part of Rodinia supercontinent, *Tectonophysics,* **375,** 325–352.

Larson, K., Small, E., Gutmann, E., Bilich, A., Axelrad, P. & Braun, J., 2008. Using GPS multipath to measure soil moisture fluctuations: initial results, *GPS Solut.,* **12,** 173–177, doi:10.1007/s10291-007-0076-6.

Le-Pichon, X., 1968. Sea-floor spreading and continental drift, *J. geophys. Res.,* **73,** 3661–3697.

Li, Q., Liu, M. & Stein, S., 2009. Spatiotemporal complexity of continental intraplate seismicity: insight from geodynamic modeling and implications for seismic hazard estimation, *Bull. seism. Soc. Am.,* **99,** 52–60, doi:10.1785/0120080005.

Lithgow-Bertelloni, C. & Silver, P., 1998. Dynamic topography, plate driving forces and the African Superswell, *Nature,* **395,** 269–272.

Liu, M., Stein, S. & Wang, H., 2011. 2000 years of migrating earthquakes in North China: how earthquakes in midcontinents differ from those at plate boundaries, *Lithosphere,* **3,** 128–132, doi:10.1130/L129.1.

Maasha, N. & Molnar, P., 1972. Earthquake fault parameters and tectonics in Africa, *J. geophys. Res.,* **77,** 5731–5743.

Malservisi, R., Dixon, T., La Femina, P. & Furlong, K., 2003. Holocene slip rate of the Wasatch fault zone, Utah, from geodetic data: earthquake cycle effects, *Geophys. Res. Lett.,* **30,** doi:10.1029/2003GL017408.

McCafrey, R. *et al.*, 2007. Fault locking, block rotation and crustal deformation in the Pacific Northwest, *Geophys. J. Int.,* **169,** 1315–1340, doi:10.111/j.1365-246X.2007.03371.x.

McClusky, S. *et al.*, 2000. GPS constraints on plate kinematics and dynamics in the eastern Mediterranean and Caucasus, *J. geophys. Res.,* **105,** 5695–5719, doi:10.1029/1996JB900351.

McClusky, S., Reilinger, R., Mahmoud, S., Ben Sari, D. & Tealeb, A., 2003. GPS constraints on Africa (Nubia) and Arabia plate motions, *Geophys. J. Int.,* **155,** 126–138.

McKenzie, D. & Parker, R., 1967. The North Pacific: an example of tectonics on a sphere, *Nature,* **216,** 1276–1280.

Midzi, V., Hlatywayo, D., Chapola, L., Kebede, F., Atakan, K., Lombe, D., Turyomurugyendo, G. & Tugume, F., 1999. Seismic hazard assessment in Eastern and Southern Africa, *Annali di Geofisica,* **42,** 1067–1083.

Milner, S., Duncan, A., Whittingham, A. & Ewart, A., 1995. Trans-Atlantic correlation of eruptive sequences and individual silicic volcanic units within the Parana-Etendeka igneous province, *J. Volc. Geotherm. Res.,* **69,** 137–157.

Minster, J., Jordan, T., Molnar, P. & Haines, E., 1974. Numerical modeling of instantaneous plate tectonics, *Geophys. J. R. astr. Soc.,* **36,** 541–576.
Modisi, M., 2000. Fault system of the southeastern boundary of the Okavango Rift, Botswana, *J. Afr. Earth Sci.,* **30,** 569–578.
Modisi, M., Atekwana, E., Kampunzu, A. & Ngwisanyi, 2000. Rift kinematics during the incipient stages of continental extension: evidence from the nascent Okavango Rift basin, northwest Botswana, *Geology,* **28,** 939–942.
Morgan, W., 1968. Raises, trenches, great faults and crustal blocks, *J. geophys. Res.,* **73,** 1959–1982.
Nocquet, J., Willis, P. & Garcia, S., 2006. Plate kinematics of Nubia-Somalia using combined DORIS and GPS solution, *J. Geod.,* **80,** 591–607, doi: 10.1007/s00190-006-0078-0.
Nyblade, A. & Langston, C., 1995. East african earthquake below 20 km and their implications for crustal structure, *Geophys. J. Int.,* **121,** 49–62.
Nyblade, A. & Robinson, S., 1994. The African superswell, *Geophys. Res. Lett.,* **21,** 765–768.
Nyblade, A. & Sleep, N., 2003. Long lasting epeirogenic uplift from mantle plumes and the origin of the Southern African Plateau, *Geochem. Geophys. Geosyst.,* **4,** 1105, doi:10.1029/2003GC000573.
Plattner, C., Malservisi, R., Dixon, T., LaFemina, P., Sella, G., Fletcher, J. & Suarez-Vidal, F., 2007. New constraints on relative motion between the Pacific Plate and Baja California microplate (Mexico) from GPS measurements, *Geophys. J. Int.,* **170,** 1373–1380.
Plattner, C., Malservisi, R., Furlong, K. & Govers, R., 2010. Development of the Eastern California Shear Zone-Walker Lane belt: the effects of microplate motion and pre-existing weakness in the Basin and Range, *Tectonophysics,* **485,** 78–84.
Prawirodirdjo, L. & Bock, L., 2004. Instantaneous global plate motion from 12 years of continuous gps observations, *J. geophys. Res.,* **109**(B8), B08405, doi:10.1029/2003JB002944.
Reeves, C., 1972. Rifting in the Kalahari, *Nature,* **254,** 408–409.
Reeves, C., 1999. Aeromagnetic and gravity features of Gondwana and their relation to continental break-up: more pieces, less puzzle, *J. Afr. Earth Sci.,* **28,** 263–277.
Reeves, C. & De Wit, M., 2000. Making ends meet in Gondwana: retracting the transforms of the Indian Ocean and reconnecting continental shear zones, *Terra Nova,* **12,** 272–280.
Reeves, C., De Wit, M. & Sahu, B., 2004. Tight reassembly of Gondwana exposes phanerozoic shears in Africa as global tectonic players, *Gondwana Res.,* **7,** 7–19.
Saada, A., 1974. *Elasticity: Theory and Applications,* Vol. 16, Pergamon Unified Engineering Series, Pergamon Press Inc., Elmsford, NY, USA.
Shewchuk, J., 1996. Triangle: engineering a 2d quality mesh generator and delaunay triangulator, in *Applied Computational Geometry: Towards Geometric Engineering,* Vol. 1148, pp. 203–222, eds Lin, M. & Manocha, D., Springer-Verlag, Berlin.
Scholz, C., Kocynski, T. & Hutchins, D., 1976. Evidence for incipient rifting in Southern Africa, *Geophys. J. R. astr. Soc.,* **44,** 135–144.
Sella, G., Dixon, T. & Mao, A., 2002. REVEL: a model for recent plate velocities from space geodesy, *J. geophys. Res.,* **107,** doi:10.1029/2000JB000033.
Sella, G., Stein, S., Dixon, T., Craymer, M., James, T., Mazzotti, S. & Dokka, R., 2007. Observation of glacial isostatic adjustment in "stable" North America with GPS, *Geophys. Res. Lett.,* **34,** L02306, doi:10.1029/2006GL027081.
Shemang, E. & Molwalefhe, L., 2011. Geomorphic landforms and tectonism along the eastern margin of the Okavango Rift Zone, Northwestern Botswana, as deduced from geophysical data, in *New Frontiers in Tectonics Research, General Problems, Sedimentary Basins, and Island Arcs,* pp. 169–182, ed. Sharkov, E., Intechopen.
Singh, M. & Hattingh, E., 2009. Collection of isoseismal maps for South Africa, *Nat. Hazards,* **50,** 403–408, doi:10.1007/s11069-008-9332-5.
Singh, M., Kijko, A. & Durrheim, R., 2009. Seismotectonic models for South Africa: synthesis of geoscientific information, problems, and the way forward, *Seism. Res. Lett.,* **80,** 71–80, doi:10.1785/gssrl.80.1.71.
Singh, M., Kijko, A. & Durrheim, R., 2011. First-order regional seismotectonic model for South Africa, *Nat. Hazards,* **52,** doi:10.1007/s11069-011-9762-3.
Smith, C., Allsopp, H., Kramers, J., Hutchinson, G. & Roddick, J., 1985. Emplacement ages of jurassic-cretaceous kimberlites by rb-sr method on phlogopite and whole rock samples, *Trans. Geol. Soc. S. Afr.,* **88,** 249–266.
Stamps, D., Calais, E., Saria, E., Hartnady, C., Nocquet, J., Ebinger, C. & Fernandes, R., 2008. A kinematic model for the east African rift, *Geophys. Res. Lett.,* **35,** L05304, doi:10.1029/2007GL032781.
Stein, S. & Gordon, R., 1984. Statistical tests of additional plate boundaries from plate motion inversions, *Earth planet. Sci. Lett.,* **69,** 401–412.
Tohver, E., D'Agrella-Filho, S. & Trindade, R., 2006. Paleomagnetic record of Africa and South America for the 1200-500 Ma interval, and evaluation of Rodinia and Gondwana assemblies, *Precambian Res.,* **147,** 193–222.
Vincenty, T., 1975. Direct and inverse solution of geodesics on the ellipsoid with application of nested equations, *Survey Rev.,* **23**(176), 88–93.
Ward, S., 1990. Pacific-North America plate motions: new results from very long baseline interferometry, *J. geophys. Res.,* **95,** 21 965–21 981.
Watkins, R., McDougall, I. & Le Roex, A., 1994. K-Ar ages of the Brandberg and Okenyenya igneous complexes, north western Nambia, *Geol. Rundsch.,* **83,** 348–356.
Wessel, P. & Smith, W.H.F., 1998. New, improved version of Generic Mapping Tools released, *EOS Trans. Amer. Geophys. U.,* **79**(47), 579.

SUPPORTING INFORMATION

Additional Supporting Information may be found in the online version of this article:

Figure S1. Residuals for the detrended time series. The star indicates the day of the Machaze earthquake.
Figure S2. Nubia IGS sites residuals for the detrended time series.
Figure S3. Comparison between the residuals for the Euler vector that better describe the motion from the time series limited to 2002–2007 (right) and the velocity field for the full time series (pol1, left).
Figure S4. Consistency test for the GPS uncertainties and residuals. The 19 sites within the most stable part of TrigNet (black and red) are plotted with error ellipses corresponding to 95 per cent, 66 per cent, and 50 per cent confidence ellipses. The sites marked in red correspond to sites with residuals larger than the corresponding confidence ellipse.
Figure S5. Motion described by Euler vectors derived from the difference of the Nubia plate vector from the colour-coded model and pol1. The residual model is compatible with a clockwise rotation of South Africa with respect to a stable Nubia plate as would be expected by a propagation of the East Africa Rift along its southern branches.
Table S1. Residual for the 'stable' TrigNet sites with at least 3 yr of data (Fig. 4) with respect to the motion described by pol1.
Table S2. Published Euler poles describing the motion of Nubia with respect to ITRF2005.
Table S3. Previously published Nubia plate angular velocities relative to ITRF2005 in cartesian coordinates with covariance matrix. Model names as referenced in Table S2.
Table S4. Residual for the Nubia Plate's IGS sites with at least 3 yr of data with respect to the motion described by pol1. (http://gji.oxfordjournals.org/lookup/supp1/doi:10.1093/gji/ggs081/-/DC1)

Please note: Oxford University Press are not responsible for the content or functionality of any supporting materials supplied by the authors. Any queries (other than missing material) should be directed to the corresponding author for the article.